Environmental Science: Atmospheres

ROYAL SOCIETY OF CHEMISTRY

PAPER

View Article Online
View Journal

Cite this: DOI: 10.1039/d5ea00164a

Health and climate impacts of policy-driven changes in open crop straw burning during China's summer harvest

Jieyu Wen,[a] Zhicheng Feng,[a] Haochen Zuo,[a] Xiaodong Xie,[a] Ying Zhou,*[b] Yiyi Wang,[c] Yang Hu[c] and Jianlin Hu *[a]

Open crop straw burning (OCSB) substantially affects the air quality in China, prompting control measures and straw-burning bans. However, long-term policy-driven impacts on air quality, public health, and climate at the national scale have received limited quantitative assessment within a unified framework. Here, we combine a localized OCSB emission inventory with paired WRF-Chem simulations (with and without OCSB) for June in 2003, 2008, 2013, 2018, and 2021 to quantify these impacts. The OCSB-induced nationwide mean $PM_{2.5}$ reached 2.82 μg m^{-3} in 2013, decreased by ~79.4% to 0.58 μg m^{-3} in 2018, and slightly rebounded in 2021. The population-weighted $PM_{2.5}$ exposure attributable to OCSB decreased by ~78.1% (from 10.48 μg m^{-3} in 2013 to 2.29 μg m^{-3} in 2021), and the non-accidental premature deaths declined by ~77.6% (from 1756; 95% confidence interval, 95% CI: 1200–2231) in 2013 to 393 (95% CI: 268–500) in 2021. The reduced OCSB emissions weakened the aerosol-induced shortwave dimming and surface cooling, indicating a diminishing compensating climate effect. Nationally, the OCSB-attributable surface shortwave net radiation (SWNET) increased from −0.64 to −0.25 W m^{-2} between 2013 and 2021, and the associated 2 m temperature (T_2) impacts weakened from −0.0056 °C to −0.0033 °C, especially over the North China Plain. Overall, our results suggest that recent reductions in OCSB emissions during the summer harvest are associated with substantial co-benefits for air quality, public health, and climate, providing national-scale evidence for refining straw-burning bans and air-pollution control strategies.

Received 10th December 2025
Accepted 23rd January 2026

DOI: 10.1039/d5ea00164a

rsc.li/esatmospheres

Environmental significance

Open crop straw burning (OCSB) is an episodic but influential emission source during China's summer harvest, yet its policy-driven evolution and integrated impacts remain incompletely quantified. Therefore, it is essential to clarify the environmental benefits of burning restrictions and their implications for air quality, public health, and climate-relevant aerosol effects. Our results show that as OCSB emissions declined, OCSB-attributable $PM_{2.5}$ exposure and premature mortality decreased markedly while weakening perturbations to surface shortwave radiation and near-surface air temperature. These findings provide quantitative evidence for refining region-specific straw-burning restrictions and supporting coordinated management of air quality–health–climate objectives.

1 Introduction

Open biomass burning (OBB), including forest fires, grassland fires, shrubland fires, and crop straw burning,[1,2] is one of the major global sources of fine particulate matter ($PM_{2.5}$) and trace gases, with far-reaching impacts on regional air quality, public health, and climate.[3–6] Aerosols emitted from OBB absorb and scatter solar radiation, thereby exerting both direct radiative forcing and indirect cloud effects.[7,8] In intensive agricultural regions, open crop straw burning (OCSB) is a particularly important source of OBB,[9,10] contributing up to 74–94% of total biomass-burning emissions.[11]

China is one of the largest agricultural producers in the world, with both cultivated area and crop residue generation ranking among the highest globally; correspondingly, the country produces approximately 600–800 Tg of crop residues each year, accounting for about 20% of the global total crop residues.[12–14] OCSB exhibits pronounced seasonal and spatial

[a]Jiangsu Key Laboratory of Atmospheric Environment Monitoring and Pollution Control, Collaborative Innovation Center of Atmospheric Environment and Equipment Technology, School of Environmental Science and Engineering, Nanjing University of Information Science & Technology, Nanjing, 210044, China. E-mail: jianlinhu@nuist.edu.cn

[b]Key Laboratory of Beijing on Regional Air Pollution Control, College of Environment Science and Engineering, Beijing University of Technology, Beijing, 100124, China. E-mail: y.zhou@bjut.edu.cn

[c]School of Energy and Environment, Anhui University of Technology, Ma'anshan 243000, China

variability, closely linked to the harvest periods of major staple crops such as wheat and rice. Previous studies have identified a distinct bimodal pattern of OCSB, with emission peaks typically occurring in summer and autumn.[15] For example, early-summer and autumn peaks have been reported in Hebei Province,[16] while spring–autumn peaks occur in Heilongjiang Province.[17] These burning activities are mainly concentrated in key grain-producing regions, including the North China Plain (NCP), the Northeast China Plain, and parts of central China, as corroborated by satellite fire detections that consistently show dense burning clusters over these areas.[15,18,19]

Intensive emissions from OCSB can have significant impacts on regional air quality, health, and climate. For regional air quality, case studies across eastern and central China consistently show that OCSB makes a major contribution to haze pollution. Zhou *et al.*[20] reported that intensive crop-residue fires over eastern Henan, southern Hebei and western Shandong produced emissions exceeding those of local anthropogenic sources during a severe haze episode and contributed 19% of surface $PM_{2.5}$ in Beijing. Cheng *et al.*[21] analyzed a severe haze episode in late May–early June 2011 across five cities (Shanghai, Hangzhou, Ningbo, Suzhou, and Nanjing) in the Yangtze River Delta (YRD) and found that biomass open burning contributed on average about 37% of $PM_{2.5}$, 70% of organic carbon and 61% of elemental carbon in these sites. They further suggested that completely banning open burning would decrease the mean $PM_{2.5}$ by ~51% in the YRD region. Luo *et al.*[22] reported that OCSB emissions contributed 25.6% of the local mean $PM_{2.5}$ concentrations in Hunan Province from 15 to 26 October 2024, with the primary organic carbon (POA) and secondary organic carbon (SOA) contents increasing by 46.2% and 62.7%, respectively. In terms of health burden, epidemiological and statistical evidence indicates that OCSB-attributable $PM_{2.5}$ enhancements are strongly associated with elevated risks of premature mortality from cardiorespiratory diseases. A county-level panel study in China estimated that an increase of 10 fire counts within 50 km is associated with a 4.79 μg m^{-3} rise in monthly mean $PM_{2.5}$ and a 1.56% increase in all-cause mortality; correspondingly, each 10 μg m^{-3} increment in $PM_{2.5}$ was linked to a 3.25% increase in mortality.[23] In addition, crop straw burning carbonaceous aerosols exert a net positive direct radiative effect at the top of the atmosphere and dim surface solar radiation, which can strengthen lower-tropospheric heating and boundary-layer stability while modifying regional temperature and circulation. In East China, WRF-Chem simulations for June 2013 showed that crop straw aerosols produced a regional mean TOA direct radiative effect of about +0.14 W m^{-2}, with local values up to +22.66 W m^{-2} and pronounced surface solar dimming.[24] During an agricultural-burning haze episode in Northeast China in November 2017, aerosol direct radiative effects reduced downward surface shortwave radiation and planetary boundary-layer height while increasing the daily mean $PM_{2.5}$ by around 16 μg m^{-3}.[25]

Since the issuance of the Measures for the Prohibition of Open Straw Burning and the Comprehensive Utilization of Straw in 1999, China has introduced a series of air pollution control policies to curb OCSB-attributable pollution. These include the 2013 Air Pollution Prevention and Control Action Plan and the 2018 Three-Year Action Plan to Fight Air Pollution, which further strengthened restrictions on OCSB and incentives for straw recycling. National OCSB activity and emission intensity declined markedly during 2013–2018, with both fire counts and pollutant emissions reduced by more than 40%.[26] However, most existing modeling studies have evaluated OCSB impacts for individual regions or short pollution episodes and often rely on global satellite-based biomass-burning emission inventories (*e.g.*, FINN), which have limited capability to detect small, scattered straw fires and can underestimate actual OCSB $PM_{2.5}$ emissions in China by up to ~85%, compared with the results obtained using localized inventories.[15,26] In addition, previous assessments have rarely performed multi-year simulations that explicitly compare conditions before and after the implementation of straw-burning bans, and they typically focus on air quality responses alone,[27,28] without jointly quantifying health burdens and climate-relevant radiative effects within a consistent framework.

In this study, we integrated a localized OCSB emission inventory with the Weather Research and Forecasting model coupled with Chemistry (WRF-Chem) to systematically quantify how OCSB emissions before and after the implementation of straw-burning control policies affect regional $PM_{2.5}$ pollution, population exposure and associated health burdens, and climate impacts over mainland China, providing a scientific basis for coordinated management of air quality, climate, and public health.

2 Methods

2.1 WRF-Chem model configuration

WRF-Chem version 3.9.1 was adopted here to examine the impacts of OCSB on air pollutants, radiation, and temperature.[29,30] It is an online-coupled regional meteorology–chemistry model based on the WRF-ARW dynamical core, in which meteorological fields, gases and aerosols are integrated on the same grid using the same transport schemes without additional temporal or spatial interpolation.[31] Photolysis and radiative transfer are calculated online, allowing aerosol–radiation–cloud interactions and feedbacks to boundary-layer meteorology and regional climate.[32] Fig. S1 summarizes the WRF-Chem modeling configuration, evaluation sites, and the four key analysis regions. The national domain (Domain 1) employed a Lambert conformal conic projection with a horizontal resolution of 36 km, covering mainland China and the surrounding regions (Fig. S1a). In addition, a 12 km one-way nested domain over the NCP and adjacent regions (Domain 2) was configured to provide higher-resolution simulations for a more detailed analysis of the OCSB-attributable changes in this hotspot region (Fig. S1b). The nested domain used the same physical and chemical parameterizations as Domain 1 (Table S1). Unless otherwise noted, the national-scale results are based on the 36 km simulations in Domain 1.

Meteorological initial and boundary conditions were taken from the National Centers for Environmental Prediction (NCEP) Final (FNL) reanalysis dataset (https://rda.ucar.edu/datasets/

ds083.2, accessed on 29 May, 2025). Anthropogenic emissions were obtained from the Multi-resolution Emission Inventory for China[33,34] version 1.4 (MEIC v1.4, http://meicmodel.org.cn, accessed on 29 May, 2025), with a spatial resolution of 0.25° × 0.25°. MEIC is a bottom-up inventory developed by Tsinghua University that compiles emissions from many detailed anthropogenic source categories, which are aggregated into five major sectors (power, industry, residential, transportation, and agriculture), and provides gridded emissions of major air pollutants and precursors over mainland China. MEIC has been widely applied in regional-air-quality, health-impact, and climate studies over China.[35,36] Simulations for 2003, 2008, 2013, and 2018 used the corresponding annual MEIC inventories, whereas the 2021 simulations used the latest available 2020 inventory. Emissions outside China were based on the MIX emission inventory[37] version 1.1 (MIX v1.1, http://www.meicmodel.org/dataset-mix, accessed on 29 May, 2025) with a spatial resolution of 0.25° × 0.25°, which provides 2010 anthropogenic emissions and was developed to support the Model Inter-Comparison Study for Asia (MICS-Asia) and the Task Force on Hemispheric Transport of Air Pollution (TF HTAP) using a mosaic of up-to-date regional emission inventories. Biogenic emissions were calculated online using the Model of Emissions of Gases and Aerosols from Nature version 2.1 (MEGAN v2.1).[38] Chemical initial and boundary conditions were provided by daily forecasts from the Community Atmosphere Model with Chemistry (CAM-Chem)[39] and the Whole Atmosphere Community Climate Model (WACCM), developed by the National Center for Atmospheric Research (NCAR).

The OCSB emission inventory used in this study was developed in-house by the Beijing University of Technology.[40,41] This inventory applies a Fire Radiative Energy (FRE)-based approach to derive the open burning proportion (OBP), enabling the estimation of the fraction of crop residues burned in the field without relying on time-consuming and expensive field investigations. FRE is retrieved from MODIS active fire products, and crop straw production is estimated from crop yield statistics combined with literature-based straw-to-grain ratios for major cereal crops (*e.g.*, wheat, maize, and rice). Emissions are calculated by multiplying the resulting burned residue mass by pollutant-specific emission factors for gaseous and particulate species, which are derived from Chinese field measurements where available and supplemented by laboratory measurements and literature values if needed. In crop straw burning emission inventories, OBP is a key parameter that can greatly affect the accuracy of emission estimates and is often prescribed as a fixed value. Zhou *et al.*[41] showed that this FRE-based OBP scheme reproduces field-investigated OBP with an overall correlation coefficient of about 0.7 and avoids the systematic under- and over-estimation (by roughly 5–30%) of national $PM_{2.5}$ emissions that arise when fixed OBP values are used across years, thereby better reflecting interannual changes in OCSB emissions. The FRE-based OBP framework also exhibits improved spatial applicability across regions and good consistency with field-investigated OBP data. In this study, OCSB emissions were released into the first vertical layer, and plume-rise parameterization was not applied, consistent with previous regional modeling work on crop straw burning in China.[42] Field observations also indicate that crop residues in China are typically burned in small, short-lived piles with limited plume rise.[43] In addition, localized measurements of the OCSB chemical composition in China remain relatively limited. In our emission inventory, we assume that the chemical composition within each straw type remains constant over time. Under this assumption, temporal variations in the OCSB emissions are primarily reflected in the total emission magnitude and the relative contributions from different straw sources.

To quantify the long-term changes in OCSB emissions and the associated impacts on air quality, health, and climate, we conducted WRF-Chem simulations for June in 2003, 2008, 2013, 2018, and 2021. These five years were selected because they represent key policy nodes in China's air pollution and straw-burning control efforts. We specifically focused on the month of June in each year, when the OCSB activity has historically been particularly important, especially in earlier high-emission years (explained in detail in Section 3.1). We designed two simulation scenarios for each month. In the SIM_OCSB scenario, the total emissions include anthropogenic, biogenic, and OCSB sources. In the SIM_noOCSB scenario, the OCSB emissions are excluded, while all other configurations remain identical. The difference between SIM_OCSB and SIM_noOCSB is interpreted as the OCSB-induced contribution to pollutant concentrations. The absolute $PM_{2.5}$ contribution from OCSB is calculated using eqn (1), and the relative contribution is defined by eqn (2).

$$\mathrm{OCSB_{mass}} = \mathrm{SIM_{OCSB}} - \mathrm{SIM_{noOCSB}} \quad (1)$$

$$\mathrm{OCSB_{contribution}} = \frac{\mathrm{OCSB_{mass}}}{\mathrm{SIM_{OCSB}}} \quad (2)$$

2.2 Observational datasets

Surface meteorological observations were obtained from the China National Meteorological Science Data Center (http://data.cma.cn/en, accessed on 1 June, 2025). Hourly surface air pollutant concentrations were acquired from the China National Environmental Monitoring Center (http://www.cnemc.cn, accessed on 1 June, 2025). Fire activity data were derived from the MODIS Collection 6.1 active fire products provided by NASA's Fire Information for Resource Management System (FIRMS; https://firms.modaps.eosdis.nasa.gov, accessed on 13 June, 2025), based on observations from the Terra and Aqua satellites. Model performance was evaluated following the statistical criteria proposed by Emery *et al.*[44,45] by comparing WRF-Chem simulations with observations for key meteorological variables and major air pollutants. Seven commonly used performance metrics were calculated, as summarized in Table S2. The model evaluation results against these surface meteorological and air quality observations are presented in SI (Text S1).

2.3 Health exposure assessment

To assess short-term $PM_{2.5}$ exposure and its evolution under emission control policies, we used the population-weighted

concentration (PWC) metric (eqn (3)) to quantify the population-average $PM_{2.5}$ exposure at the provincial level.

$$\mathrm{PWC} = \frac{\sum_i C_i \times P_i}{\sum_i P_i} \quad (3)$$

where i denotes the grid cell within the model domain, C_i is the $PM_{2.5}$ concentration in grid cell i, and P_i is the corresponding population. Gridded population data were obtained from the WorldPop database (http://www.worldpop.org, accessed on 14 August, 2025) using the China 2018 UN-adjusted dataset[46] and adjusted to match the national total population estimates reported in the China Statistical Yearbook 2019. For health impact calculations, we used the 2018 population distribution and baseline mortality rates for all simulation years (2003, 2008, 2013, 2018 and 2021). This fixed-population setup allowed differences in OCSB-attributable health burdens between years to be driven mainly by changes in OCSB-induced $PM_{2.5}$ rather than by demographic or baseline mortality changes.

We applied an exposure-response-based Health Impact Assessment (HIA) model to estimate non-accidental all-cause premature deaths attributable to short-term increases in $PM_{2.5}$ induced by OCSB (eqn (4)–(7)). The exposure–response coefficient (β) was adopted from Chen *et al.*,[47] who conducted a time-series analysis for 272 Chinese cities; Chen *et al.* reported the effect as a percentage increase in mortality risk per 10 μg m^{-3} increase in $PM_{2.5}$, which we converted into the corresponding log-linear coefficient β used in eqn (5) and (6).

$$\Delta C_{t,i} = C_{t,i}^{\mathrm{SIM_{OCSB}}} - C_{t,i}^{\mathrm{SIM_{noOCSB}}} \quad (4)$$

$$\mathrm{RR}_{t,i} = \exp\left(\beta \frac{\Delta C_{t,i}}{10}\right) \quad (5)$$

$$\mathrm{AF}_{t,i} = 1 - \exp\left(-\beta \frac{\Delta C_{t,i}}{10}\right) \quad (6)$$

$$\Delta M_{t,i} = y_{0,\mathrm{daily}} P_i \mathrm{AF}_{t,i}, \quad y_{0,\mathrm{daily}} = \frac{y_{0,\mathrm{annual}}}{365} \quad (7)$$

where $\Delta C_{t,i}$ denotes the OCSB-induced increment in the $PM_{2.5}$ concentration for grid cell i on day t; $\mathrm{RR}_{t,i}$ is the relative risk of mortality associated with the OCSB-induced $PM_{2.5}$ increment $\Delta C_{t,i}$, based on a log-linear coefficient per 10 μg m^{-3} increase in $PM_{2.5}$; $\mathrm{AF}_{t,i}$ is the attributable fraction of deaths due to the OCSB-induced $PM_{2.5}$ increment, $\Delta C_{t,i}$; $\Delta M_{t,i}$ represents the number of attributable deaths per day; y_0 is the baseline non-accidental mortality rate; and P_i is the population in grid cell i.

3 Results and discussion

3.1 Spatiotemporal changes in OCSB-induced emissions

Fig. 1a shows the monthly fractions of annual OCSB-$PM_{2.5}$ emissions for 2003, 2008, 2013, 2018, and 2021. All years exhibit pronounced seasonal peaks. Before 2013, June consistently accounts for the largest share, with June emissions in 2013 reaching 309.7 Gg (Fig. 1b), substantially higher than those in 2003 (193.8 Gg) and 2008 (282.6 Gg), indicating that the intensive burning during the summer harvest season largely controls annual OCSB-$PM_{2.5}$ emissions. However, the seasonal peak had shifted to earlier months by 2018. June emissions decreased by ~77.5% to 69.8 Gg, and March–April emissions became the largest monthly contributors (Fig. S2). The monthly distribution for 2021 further confirms this transition, with April emerging as the new peak month rather than early summer. These results indicate that, under policy intervention, the seasonal pattern of national OCSB-$PM_{2.5}$ emissions has been substantially reshaped, with the dominant peak shifting from June to early spring due to a combination of sharply reduced June emissions and substantially enhanced April emissions.

We analyzed the spatiotemporal patterns of June OCSB-$PM_{2.5}$ emissions for the selected years. Overall, high-emission areas are consistently concentrated over major grain-producing regions, particularly the NCP and adjacent regions (Fig. 1c), including regions such as Henan, Shandong, northern Jiangsu, and northern Anhui. This aggregation pattern is evident in all years, but the spatial extent and intensity of emissions vary over time. In 2018 and 2021, the high-emission areas shrank substantially, and only the localized hotspots remained, with markedly reduced intensities. In contrast, the emission signals in the Northeast China Plain and the Middle–Lower Yangtze Plain are generally weaker and more scattered in June. This may be related to differences in regional crop planting structures and harvest calendars, as discussed in Section 3.4. Fig. 1d shows that the OCSB emissions in earlier years (*e.g.*, 2003 and 2008) display sharp peaks concentrated in early to mid-June, with maximum daily totals reaching 40.2 and 54.7 Gg. By 2018 and 2021, such short-term intensive burning in June had largely disappeared. Daily emissions stay at relatively low levels for most of the month, and the maximum daily peaks drop significantly to 8.2 and 9.1 Gg, indicating a pronounced reduction in short-lived extreme burning in episodes June over major wheat-harvest regions.

We further corroborated these emission patterns using MODIS active fire detections. Analysis of fire counts and locations (Fig. S3) captures the interannual variability in both the timing and spatial distribution of active fires associated with open burning. In all years, fire hotspots in June exhibit strong spatial clustering, with the NCP consistently serving as the core hotspot region (Fig. S3a), consistent with intensive wheat residue burning during the summer harvest. Meanwhile, fire detections are generally more dispersed and show a scattered pattern over the Northeast China Plain and the Middle–Lower Yangtze Plain. The fire activity increased from 2003 to 2013, reaching in 2013 with 11 891 detected fires, followed by a sharp decline. By 2018, the number of detected fires had decreased by ~60.4% to 4706. Before 2013, pronounced fire outbreaks frequently occurred in early to mid-June (Fig. S3b), closely aligning with the peaks in the OCSB emissions. Taken together, the post-2013 decline in both the MODIS fire activity and inventory-based emissions across mainland China, with the most pronounced reductions recorded over the NCP and adjacent wheat-harvest regions, is consistent with the strengthening of straw-burning restrictions in recent years.

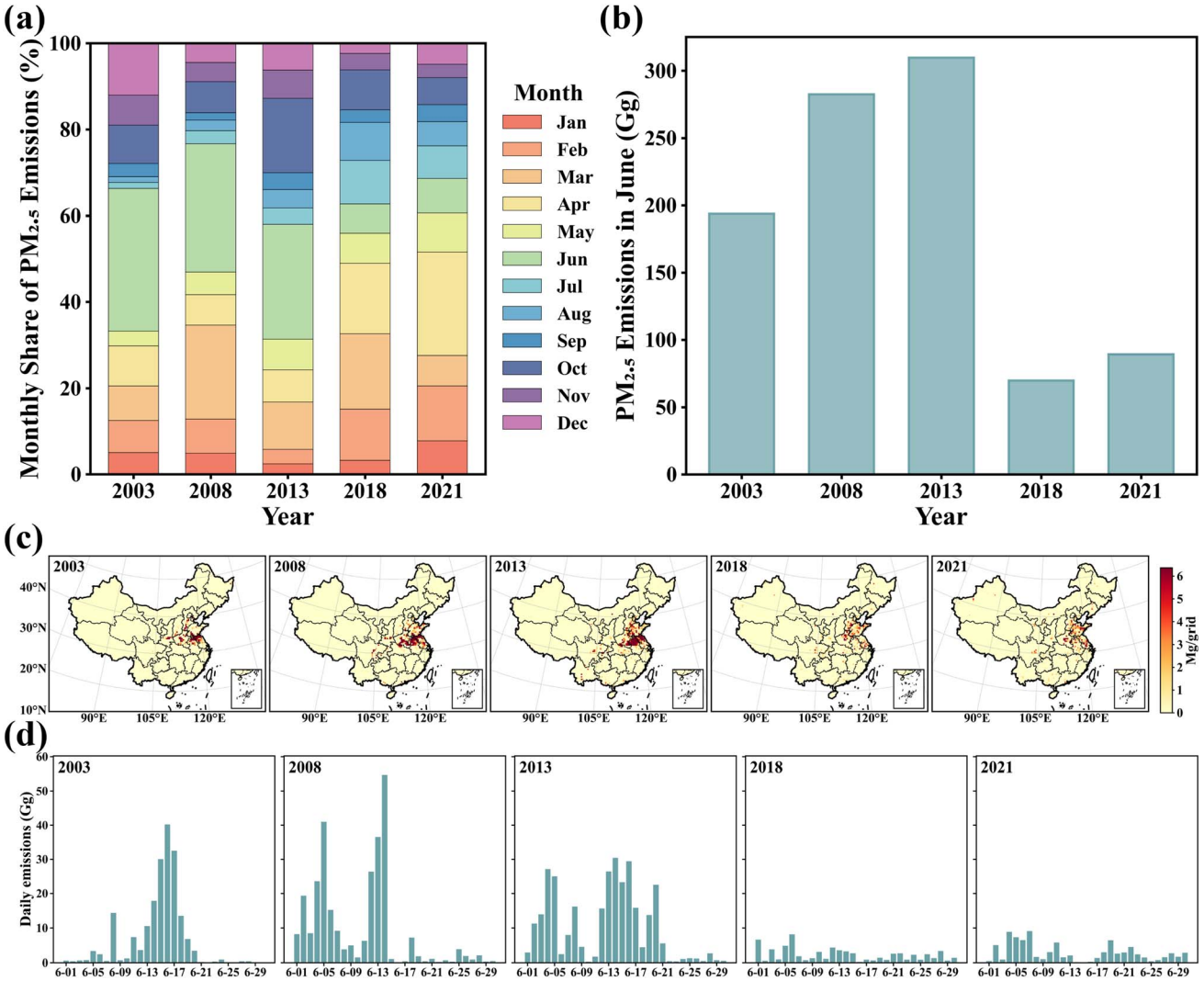

Fig. 1 OCSB $PM_{2.5}$ emissions over China in 2003, 2008, 2013, 2018, and 2021. (a) Monthly shares of annual $PM_{2.5}$ emissions from OCSB. (b) Nation-wide total emissions in June. (c) Mean spatial distribution of $PM_{2.5}$ emissions in June. (d) Nation-wide daily total $PM_{2.5}$ emissions in June.

3.2 Impacts of OCSB controls on air quality and health burden

Fig. 2 summarizes the national OCSB-induced $PM_{2.5}$ concentration contribution, population-weighted exposure, and short-term premature mortality. Overall, the national mean OCSB-induced $PM_{2.5}$ contribution increased markedly in the early years, reaching 2.82 μg m^{-3} in 2013 (Fig. 2a), compared with 1.82 μg m^{-3} in 2003. In 2013, the median and interquartile range of the daily China-average contributions in June were also the largest, with longer whiskers, indicating higher typical daily contributions and stronger day-to-day variability during June. By 2018, the mean contribution dropped by 79.4% to 0.58 μg m^{-3}, and the box and whiskers narrowed markedly, reflecting both lower contributions and reduced day-to-day variability. In 2021, the mean slightly rebounded to 0.62 μg m^{-3}, but the median remained low and the spread stayed limited, suggesting that the OCSB-attributable $PM_{2.5}$ contributions remained generally constrained nationwide.

Fig. S7 presents the spatial patterns and temporal evolution of the OCSB-induced $PM_{2.5}$ mass contributions and the relative contributions in June. At the national scale, the largest absolute contributions are consistently concentrated over the southern NCP and adjacent regions. In June 2003, a pronounced hotspot emerges at the junction of Jiangsu, Anhui, Shandong, and Henan, with a maximum contribution of 200.18 μg m^{-3} (Fig. S7a). The high-contribution areas further expand in 2008 and 2013, with maximum values of 174.40 μg m^{-3} and 200.28 μg m^{-3}, respectively. By 2018 and 2021, these hotspots shrink markedly, and the maxima decrease to ~30 μg m^{-3}, with only limited areas retaining notable contributions, reflecting the effectiveness of the strengthened OCSB control measures in the southern NCP and adjacent regions after 2013. Meanwhile, the absolute contributions peak over the southern NCP, whereas the relative contributions remain spatially scattered in other grain-producing regions in some years, suggesting that the OCSB impacts exhibit regional heterogeneity.

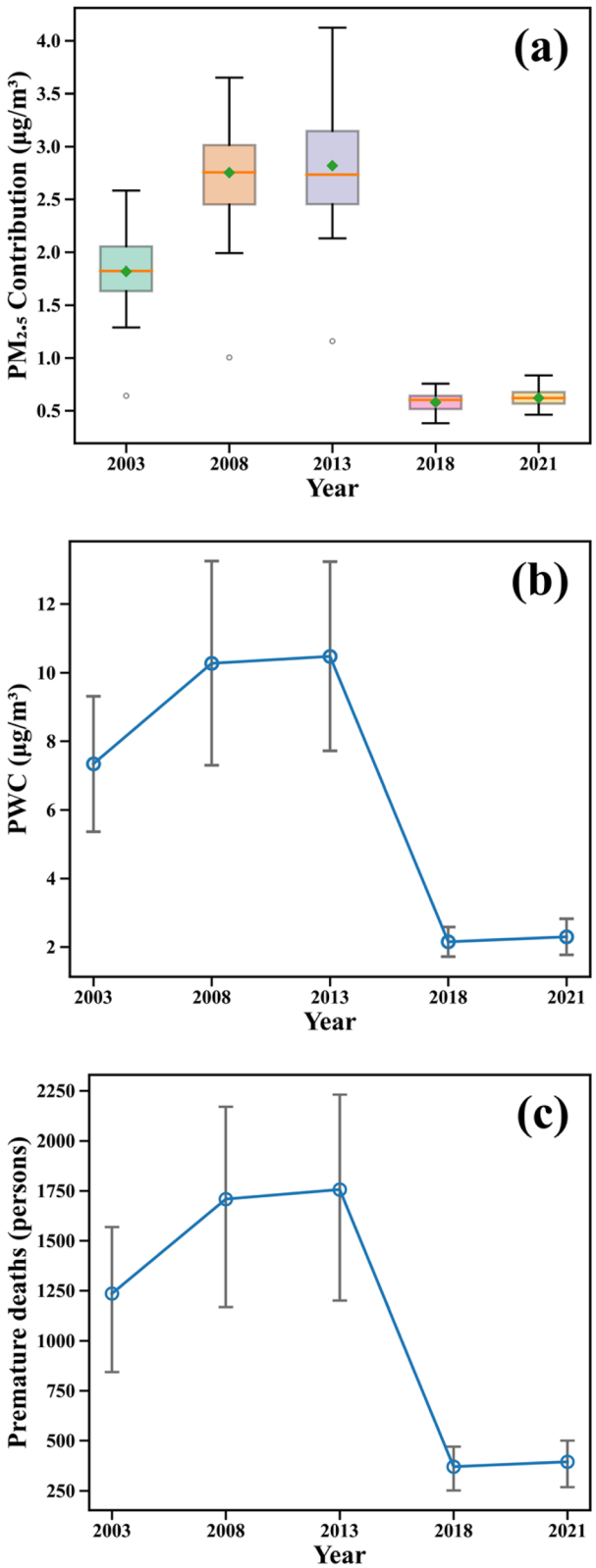

Fig. 2 OCSB impacts on $PM_{2.5}$, population-weighted $PM_{2.5}$ (PWC), and premature mortality in June for 2003, 2008, 2013, 2018, and 2021. (a) National mean $PM_{2.5}$ in June attributable to OCSB. (b) National ΔPWC (vertical bars are standard errors (SEs) across provinces.). (c) National short-term premature deaths attributable to OCSB, estimated from $\Delta PM_{2.5}$ using a lag 0–1 concentration–response function; vertical bars show the 95% confidence interval propagated from the β coefficient.

To characterize the chemical composition of the OCSB-attributable $PM_{2.5}$, we further quantified the contributions of five major aerosol components, namely organic carbon (OC), elemental carbon (EC), sulfate (SO_4^{2-}), nitrate (NO_3^-), and ammonium (NH_4^+) (Fig. S8). Among these five components, OC contributes the largest fraction, followed by secondary inorganic species (SO_4^{2-}, NO_3^-, and NH_4^+), while EC contributes a smaller but non-negligible portion. Although the absolute concentrations of all five components decrease markedly after 2013 in response to strengthened control measures, their fractional composition within the OCSB-attributable $PM_{2.5}$ remains broadly similar from 2003 to 2021, with no pronounced interannual changes.

Changes in population-weighted $PM_{2.5}$ exposure attributable to OCSB (PWC; Fig. 2b) closely track the national mean OCSB-induced $PM_{2.5}$ contribution. The PWC increased from 7.34 μg m^{-3} in 2003 to 10.48 μg m^{-3} in 2013, then dropped sharply to 2.15 μg m^{-3} in 2018 and modestly rebounded to 2.29 μg m^{-3} in 2021. Overall, the PWC in 2021 decreased by ~78.1% relative to that in 2013. The vertical bars in Fig. 2b represent the standard error across provinces. The largest standard errors are obtained in the early years, and much smaller errors are obtained in 2018 and 2021, suggesting reduced cross-provincial variability in OCSB-attributable exposure as the overall exposure declined. Fig. S9 further shows that the remaining exposure burden is concentrated in major grain-producing provinces (Hebei, Shandong, Henan, Anhui, and Jiangsu), consistent with their persistent OCSB activity during harvest seasons.

Fig. 2c shows that the temporal evolution of OCSB-attributable short-term non-accidental all-cause premature deaths closely follows the PWC. Estimated deaths peaked at 1756 (95% CI: 1200–2231) in 2013 and declined to 393 (95% CI: 268–500) in 2021, representing a 77.6% reduction. This temporal evolution closely mirrors the change in the OCSB-attributable PWC, indicating that the decrease in exposure translated into substantial short-term health benefits. Spatially, the largest absolute reductions are concentrated in eastern and central China, where the OCSB-attributable exposure is the highest.

3.3 Impacts on surface radiation and near-surface air temperature

Fig. 3 illustrates the interannual variations in June OCSB-induced surface shortwave net radiation (SWNET) and 2 m air temperature (T_2) over China and four key regions (East China (EC), Central China (CC), North China (NC), Northeast China (NEC)). The provincial composition of each region is listed in Table S4. Overall, OCSB leads to surface shortwave dimming, with pronounced regional contrasts (Fig. 3a). The national-mean SWNET reduction is largest in 2013 (−0.60 W m^{-2}). Regionally, the dimming reaches −2.81 W m^{-2} in CC and −1.74 W m^{-2} in EC; the changes in NC and NEC are close to the national mean. In 2018, the OCSB-induced dimming weakens substantially, with regional means spanning −0.10 to −0.48 W m^{-2}. Notably, EC shows a stronger SWNET reduction in 2021

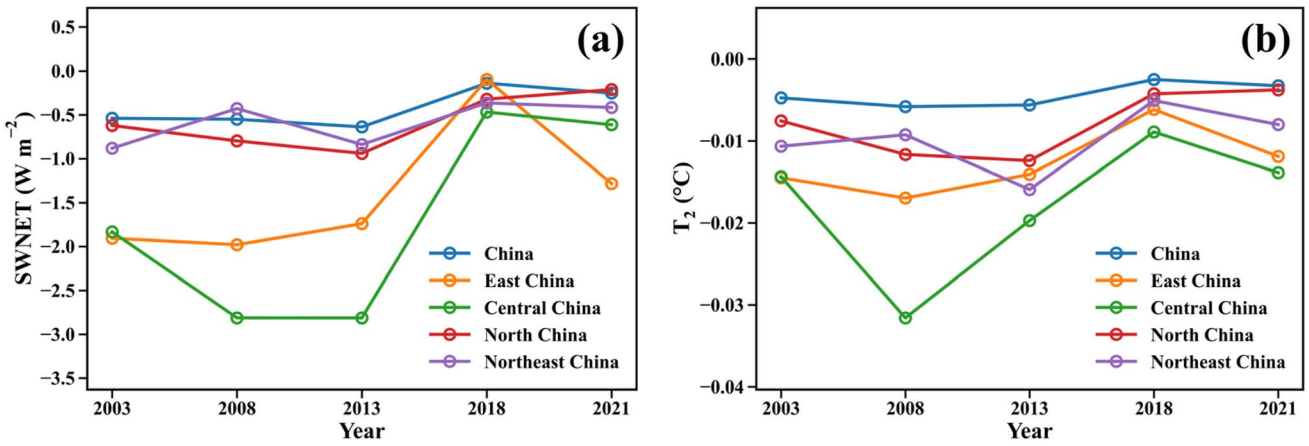

Fig. 3 Regional-mean OCSB-attributable radiative and temperature responses in June for China and its four subregions (East China, Central China, North China, and Northeast China) in 2003, 2008, 2013, 2018, and 2021. (a) Surface net shortwave radiation (SWNET). (b) 2 m air temperature (T_2).

(-1.30 W m^{-2}), consistent with the continued presence of June OCSB emission hotspots (Fig. 1c).

Fig. 3b shows the OCSB-induced change in the mean T_2 in June. The T_2 response is negative in all years, indicating an overall cooling associated with OCSB. The national mean cooling is the strongest in 2008 (-0.0058 °C) and the weakest in 2018 (-0.0025 °C), consistent with a weakened temperature response in the later, lower-emission years. Regionally, CC exhibits the largest cooling, reaching -0.0316 °C in 2008, whereas EC, NC, and NEC show much smaller changes. Overall, the regional contrasts highlight pronounced heterogeneity in the OCSB-induced temperature response. Although SWNET and T_2 generally co-vary across years, their peak responses do not necessarily coincide (*e.g.*, Central China shows the strongest SWNET dimming in 2013 but the strongest cooling in 2008). This mismatch suggests that, in addition to the radiative perturbation, the T_2 response may be modulated by year-to-year variability in regional meteorology and land–atmosphere coupling.

Based on the above analyses, we find that the southern NCP and adjacent regions exhibit the greatest and most spatially coherent changes in the OCSB-attributable impacts in June between 2013 and 2021. Therefore, we conducted additional 12 km one-way nested simulations over the NCP and adjacent regions (Domain 2) to increase the spatial resolution and provide a focused high-resolution assessment for this hotspot region. Fig. 4 displays the spatial differences in the OCSB-attributable impacts in June between 2021 and 2013 (2021 minus 2013) over China (left panels) and the NCP and adjacent regions (right panels). We find that changes in the OCSB-attributable impacts in June are most pronounced over the southern NCP, particularly in the border region between Jiangsu, Anhui, Shandong, and Henan. In this hotspot region, the OCSB-attributable $PM_{2.5}$ contribution in June decreases markedly, with a regional mean reduction of 9.70 μg m^{-3} and local decreases exceeding 100 μg m^{-3}. Compared with 2013, the aerosol perturbation associated with the OCSB emissions in June is weaker in 2021, and the resulting difference in the OCSB-attributable SWNET response over the NCP and adjacent regions shows a regional-mean increase of 2.34 W m^{-2}, indicating a weakened shortwave dimming effect. By contrast, the OCSB-attributable T_2 response shows a small and spatially heterogeneous difference, with a regional-mean change of only +0.007 °C over the NCP and adjacent regions, suggesting that OCSB has only a minor influence on near-surface temperature in June when averaged over this area.

3.4 Discussion

Compared with previous studies, this work provides a national-scale assessment of OCSB impacts spanning 2003–2021 during the summer harvest season, based on simulations for five specific years. Earlier regional modeling studies based on WRF-Chem or CMAQ have shown that OCSB can increase the $PM_{2.5}$ concentrations by 20–40% over the NCP or CC during specific years or pollution episodes, identifying OCSB as an important driver of heavy haze events.[22] Our results confirm this conclusion at the national scale and further demonstrate that the contribution of OCSB to $PM_{2.5}$ in June is substantially larger in high-emission years and becomes markedly lower in other (later) years during periods of strengthened controls. This pattern is qualitatively consistent with the work of Huang *et al.*,[26] who reported an approximately 47% reduction in OCSB-attributable $PM_{2.5}$ emissions due to straw-burning bans. Notably, we observe a modest rebound in OCSB emissions in June from 2018 to 2021. Considering both the national OCSB emissions in June and the nationwide mean OCSB-attributable $PM_{2.5}$ contribution, we observe a modest increase in 2021 relative to 2018. However, this rebound is primarily driven by enhanced signals over Shandong, Jiangsu, Anhui, and Henan in the southern NCP and, therefore, does not imply a uniform nationwide resurgence. This rebound in certain regions is consistent with recent studies and suggests spatially heterogeneous enforcement and adaptive burning behavior. He *et al.*[48] reported renewed increases in fire activity over provinces such

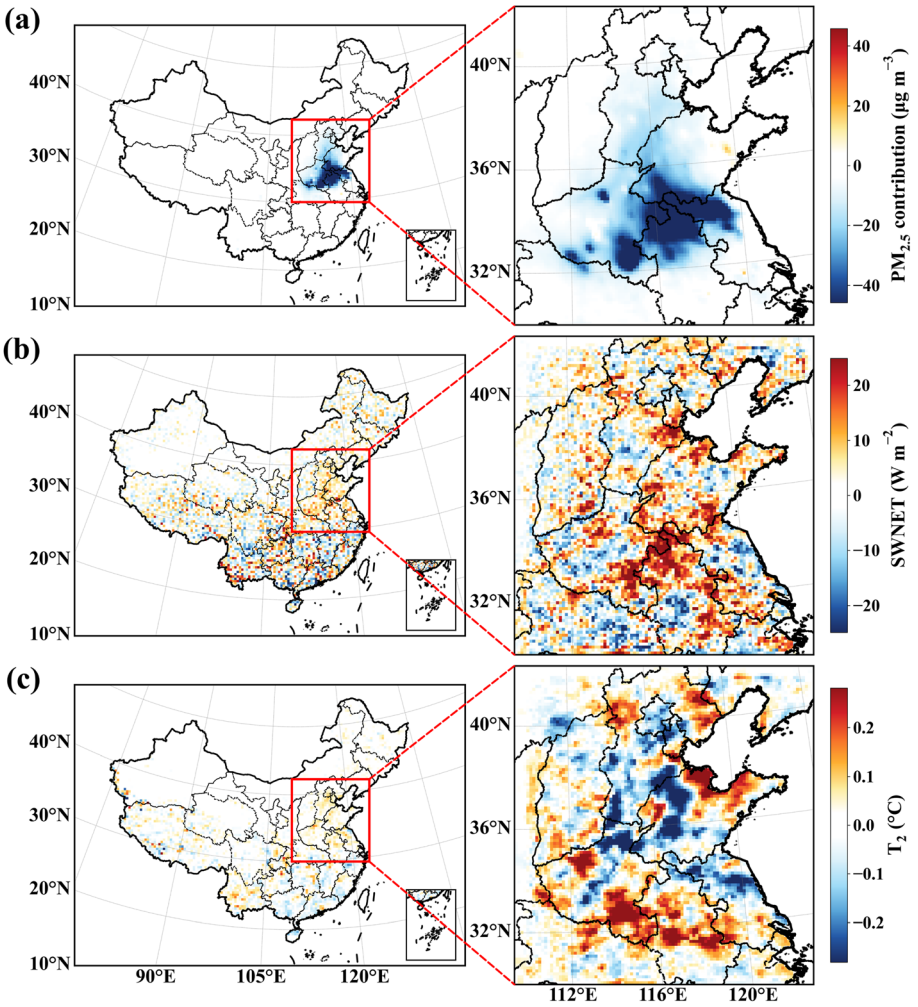

Fig. 4 Spatial differences in the mean OCSB-attributable $PM_{2.5}$ in June (a), SWNET (b), and T_2 (c) between 2021 and 2013 over China in domain 1 (36 km, left) and the nested domain 2 (12 km, right) covering the NCP and adjacent regions.

as Guangxi and Hunan during 2021–2023, reflecting spatial heterogeneity in local enforcement. Lv *et al.*[49] found rising fractions of nocturnal burning in April prior to spring ploughing in central and northeastern China, while Liang *et al.*[50] highlighted insufficient mechanization, weakened subsidies for straw utilization, and economic pressures as key drivers undermining control effectiveness.

Additionally, the relatively weaker and more spatially dispersed OCSB emissions and impacts observed in June over the Northeast China Plain and the middle–lower Yangtze River Plain (Fig. 1c and S7) do not imply that the OCSB influences in these regions are negligible on an annual basis. Instead, this pattern more plausibly reflects regional differences in cropping systems, harvest calendars, and straw disposal practices. Satellite-based fire detections and emission inventories consistently show that OCSB is strongly regulated by agricultural seasonality in China. In the main NC production belt dominated by winter wheat–summer maize rotation, hotspots and emissions peak sharply in May–June following wheat harvest, with a secondary peak observed in September–October associated with maize harvest. By contrast, the Northeast China Plain exhibits more pronounced fire and emission peaks during spring land preparation (April) and after the autumn harvest (late October).[15] During the summer harvest season in June, the Northeast China Plain is dominated by single-cropping systems with maize and soybean as the primary crops. Consequently, the OCSB-attributable signals in June tend to be more scattered and localized, reflecting the influence of region-specific cropping systems and agricultural calendars.[51] This contrasts with the continuous high-emission belts observed during winter wheat harvest in the southern NCP. For the Middle–Lower Yangtze Plain, rice–wheat rotation systems imply a potential open-burning window during the May–June wheat-harvest period.[52] Meanwhile, recent control strategies in many provinces have increasingly combined open-burning bans with measures promoting in-field straw return and off-field comprehensive utilization.[53] Previous studies have shown that integrated control strategies, when supported by straw utilization systems and fiscal incentives, can substantially reduce the frequency and intensity of open straw burning, thereby contributing to improved air quality.[23] This progress is also strongly influenced by farmers' access to and adoption of straw

disposal technologies, such as mechanical shredding and deep plowing, as well as their cost-benefit considerations.[54]

Nationwide multicity epidemiological studies in China have reported consistent associations between short-term $PM_{2.5}$ exposure and all-cause, as well as cardiorespiratory mortality, supporting the use of concentration–response functions to quantify acute health impacts attributable to OCSB-induced $PM_{2.5}$.[47,55] In this study, the close co-variation between OCSB-attributable premature deaths and the PWC (Fig. 2) underscores exposure as the dominant driver of the short-term health burden in our framework. The sharp decline from the 2013 peak to 2021 indicates that reduced OCSB-attributable $PM_{2.5}$ exposure translated into substantial acute health benefits during the harvest season. Because we applied a fixed 2018 population distribution and baseline mortality rates across all years, interannual differences in premature deaths predominantly reflect the changes in the OCSB-induced $PM_{2.5}$ rather than demographic shifts. Although we did not derive provincial premature-death estimates, the provincial PWC patterns suggest that health benefits are likely concentrated in provinces with the largest reductions in OCSB-attributable exposure.

Our findings on surface radiation and temperature feedbacks further highlight the climate co-benefits of OCSB emission reductions. Previous studies have shown that organic carbon and black carbon from crop residue burning and other biomass fires can attenuate surface shortwave radiation, enhance atmospheric heating, and modify boundary layer structure, thereby inducing cooling responses at regional scales.[56–58] Although we do not consider brown carbon in this study, which may lead to underprediction of the atmospheric heating of OCSB, our results consistently indicate that during high-emission years (*e.g.*, 2013), OCSB-induced negative shortwave radiative forcing and surface cooling are most pronounced over central China and the southern NCP. As OCSB emissions decline, associated aerosol loadings decrease, leading to weaker negative shortwave forcing and a reduced cooling effect. For example, over the NCP and adjacent regions, OCSB-attributable SWNET and T_2 are higher in 2021 than in 2013, consistent with reduced radiative dimming and a weaker cooling response in the lower-emission year.

A few limitations exist in this study. First, we apply a fixed baseline mortality rate and do not account for heterogeneity in vulnerability across regions, age groups, and health status, nor for potential changes in underlying mortality patterns. The assessment focuses solely on short-term acute exposure, without accounting for chronic effects or interactions among multiple pollutants and temperature, and thus, it likely provides conservative estimates of health risks. Second, aerosol–radiation–boundary layer feedbacks are highly complex, and our representation may not fully capture processes such as convective adjustments and cloud responses, leading to potential underestimation of meteorological feedbacks. Third, the accuracy of the results in assessing biomass burning impacts on air quality, health and climate is affected by the uncertainties in biomass burning emission estimates. We use state-of-the-art OCSB emission estimates in this study by combining the FRE-based OBP scheme with crop straw production from crop yield statistics and localized emission factors from Chinese field measurements. Although the emission estimates have been validated previously,[40,41] uncertainties still exist, which are primarily derived from activity data (*e.g.*, burned area, fuel load, combustion efficiency) and emission factors that vary significantly with vegetation type, fire intensity, and meteorological conditions. These emission uncertainties propagate through air quality models, leading to biased simulations of pollutant concentrations. Uncertainties also arise from the simplified vertical allocation of OCSB emissions. As described in Section 2.1, all OCSB emissions in our configuration are injected into the first model layer without a plume-rise parameterization. This treatment may slightly overestimate the near-source surface $PM_{2.5}$ concentrations and shortwave dimming while potentially underestimating elevated and downwind impacts. However, because the same injection approach is applied consistently across all years and scenarios, this simplification is unlikely to substantially affect the overall multi-year patterns reported in this work. Finally, we lack quantitative indicators of policy stringency and enforcement, making it difficult to attribute observed changes in OCSB emissions and air quality unambiguously to specific measures. Additionally, concurrent socioeconomic dynamics may modulate residue burning activities and pollution levels.

4 Conclusions

We present a unified national-scale quantification of the integrated impacts of OCSB during China's summer harvest over 2003–2021 under policy-driven changes. We find a pronounced decline in OCSB emissions in June and corresponding reductions in OCSB-attributable $PM_{2.5}$ enhancements, population-weighted $PM_{2.5}$ exposure, and short-term $PM_{2.5}$-related premature mortality at the national scale, indicating substantial air-quality improvements and significant health benefits during the harvest season in recent years. Consistent with these improvements, OCSB-attributable surface shortwave dimming and near-surface cooling weaken over time, indicating a reduced climate-relevant influence in later years.

The southern NCP remains the dominant hotspot of OCSB influence across metrics. A modest rebound from 2018 to 2021 is observed, primarily concentrated over Jiangsu, Anhui, Shandong, and Henan, rather than reflecting a uniform nationwide resurgence, implying spatially heterogeneous enforcement and adaptive burning behavior. Overall, our results identify OCSB as a major policy-relevant source whose adverse air quality, health, and radiative impacts can be substantially mitigated through strengthened and regionally targeted controls, together with sustained incentives for straw utilization. Future studies could better explain the 2018–2021 rebound and regional heterogeneity by integrating quantitative proxies of policy enforcement with socioeconomic constraints on straw utilization. They should also explicitly characterize the day–night variability of burning and potential timing shifts under the combined influence of regulation and meteorology to identify adaptive burning behavior and its implications for emissions and exposure. In addition, health assessments would benefit from

incorporating age- and cause-specific baseline mortality and extending impact quantification from short-term acute exposure to long-term exposure effects. To constrain the climate-relevant responses more robustly, future work should improve and observationally evaluate aerosol optical properties, including brown carbon absorption, and better constrain aerosol–cloud interactions, thereby strengthening attribution and co-benefit estimates.

Author contributions

Conceptualization: J. H.; methodology: J. W., J. H., Y. W.; investigation: J. W., Z. F., X. X.; formal analysis: J. W.; data curation: J. W., Y. Z., Y. W., Y. H.; resources: Y. Z., J. H.; visualization: J. W., H. Z.; writing – original draft: J. W.; writing – review & editing: J. W., J. H., Y. Z.; supervision: J. H., Y. Z.; funding acquisition: J.H.

Conflicts of interest

The authors declare that they have no known competing financial interests.

Data availability

Data will be made available on request.

Supplementary information (SI): one supporting text (Text S1), nine figures (Fig. S1–S9), and four tables (Tables S1–S4). Text S1 and Fig. S4–S6 provide the WRF-Chem model evaluation against the surface meteorological variables and major air pollutants across 74 cities. Fig. S2 and S3 summarize the OCSB-induced $PM_{2.5}$ emissions and MODIS active-fire detections. Fig. S7–S9 present the OCSB-attributable $PM_{2.5}$ impacts (absolute and relative), chemical composition of OCSB-attributable $PM_{2.5}$, and provincial population-weighted $PM_{2.5}$ concentrations. Tables S1–S4 provide the WRF-Chem model configuration, definitions and formulas of the statistical metrics, list of the 74 evaluation cities, and definition of the four analysis regions with province lists, respectively. See DOI: https://doi.org/10.1039/d5ea00164a.

Acknowledgements

This study was supported by the National Key Research and Development Program of China (2022YFC3701000, task 5), the National Natural Science Foundation of China (42021004, 42277095), and the Qing Lan Project of Colleges and Universities in Jiangsu Province.

References

1 X. Qiu, L. Duan, F. Chai, S. Wang, Q. Yu and S. Wang, Deriving high-resolution emission inventory of open biomass burning in China based on satellite observations, *Environ. Sci. Technol.*, 2016, **50**, 11779–11786.

2 G. R. Van der Werf, J. T. Randerson, L. Giglio, G. Collatz, M. Mu, P. S. Kasibhatla, D. C. Morton, R. DeFries, Y. V. Jin and T. T. van Leeuwen, Global fire emissions and the contribution of deforestation, savanna, forest, agricultural, and peat fires (1997–2009), *Atmos. Chem. Phys.*, 2010, **10**, 11707–11735.

3 S. Akagi, R. J. Yokelson, C. Wiedinmyer, M. J. Alvarado, J. S. Reid, T. Karl, J. D. Crounse and P. O. Wennberg, Emission factors for open and domestic biomass burning for use in atmospheric models, *Atmos. Chem. Phys.*, 2011, **11**, 4039–4072.

4 M. O. Andreae and P. Merlet, Emission of trace gases and aerosols from biomass burning, *Glob. Biogeochem. Cycles*, 2001, **15**, 955–966.

5 J. Chen, C. Li, Z. Ristovski, A. Milic, Y. Gu, M. S. Islam, S. Wang, J. Hao, H. Zhang, C. He, H. Guo, H. Fu, B. Miljevic, L. Morawska, T. Phong, Y. F. Lam, G. Pereira, A. Ding, X. Huang and U. C. Dumka, A review of biomass burning: Emissions and impacts on air quality, health and climate in China, *Sci. Total Environ.*, 2017, **579**, 1000–1034.

6 S. Szopa, V. Naik, B. Adhikary, P. Artaxo, T. Berntsen, W. D. Collins, S. Fuzzi, L. Gallardo, A. Kiendler-Scharr and Z. Klimont, Short-Lived Climate Forcers (Chapter 6), *IPCC 2021: Climate Change 2021: the Physical Science Basis. Contribution of Working Group I to the Sixth Assessment Report of the Intergovernmental Panel on Climate Change*, 2023, pp. 817–922.

7 P. Crippa, R. Sullivan, A. Thota and S. Pryor, Evaluating the skill of high-resolution WRF-Chem simulations in describing drivers of aerosol direct climate forcing on the regional scale, *Atmos. Chem. Phys.*, 2016, **16**, 397–416.

8 M. Z. Jacobson, Strong radiative heating due to the mixing state of black carbon in atmospheric aerosols, *Nature*, 2001, **409**, 695–697.

9 X. Li, S. Wang, L. Duan, J. Hao, C. Li, Y. Chen and L. Yang, Particulate and trace gas emissions from open burning of wheat straw and corn stover in China, *Environ. Sci. Technol.*, 2007, **41**, 6052–6058.

10 Y. Qin and S. Xie, Historical estimation of carbonaceous aerosol emissions from biomass open burning in China for the period 1990–2005, *Environ. Pollut.*, 2011, **159**, 3316–3323.

11 K. Mehmood, Y. Wu, L. Wang, S. Yu, P. Li, X. Chen, Z. Li, Y. Zhang, M. Li and W. Liu, Relative effects of open biomass burning and open crop straw burning on haze formation over central and eastern China: modeling study driven by constrained emissions, *Atmos. Chem. Phys.*, 2020, **20**, 2419–2443.

12 J. Chen, Y. Gong, S. Wang, B. Guan, J. Balkovic and F. Kraxner, To burn or retain crop residues on croplands? An integrated analysis of crop residue management in China, *Sci. Total Environ.*, 2019, **662**, 141–150.

13 D. Jiang, D. Zhuang, J. Fu, Y. Huang and K. Wen, Bioenergy potential from crop residues in China: Availability and distribution, *Renew. Sustain. Energy Rev.*, 2012, **16**, 1377–1382.

14 X. Zhao, R.-C. Li, W.-X. Liu, W.-S. Liu, Y.-H. Xue, R.-H. Sun, Y.-X. Wei, Z. Chen, R. Lal and Y. P. Dang, Estimation of crop residue production and its contribution to carbon

neutrality in China, *Resour. Conserv. Recycl.*, 2024, **203**, 107450.
15 X. Huang, M. Li, J. Li and Y. Song, A high-resolution emission inventory of crop burning in fields in China based on MODIS Thermal Anomalies/Fire products, *Atmos. Environ.*, 2012, **50**, 9–15.
16 Y. Zhou, Y. Zhang, X. Xing, X. Xia and J. Lang, Impacts of emissions from crop residue open burning in Hebei on the air quality of the Beijing-Tianjin-Hebei region, *J. Beijing Univ. Technol.*, 2022, **48**, 1056–1068.
17 B. Li, Z. Xu, B. Liu, Z. Zhang, W. Qiu and W. Wang, Development of a finer-resolution multi-year emission inventory for open biomass burning in Heilongjiang Province, China, *Sci. Rep.*, 2024, **14**, 29969.
18 Y. Zhuang, R. Li, H. Yang, D. Chen, Z. Chen, B. Gao and B. He, Understanding temporal and spatial distribution of crop residue burning in China from 2003 to 2017 using MODIS data, *Remote Sens.*, 2018, **10**, 390.
19 L. Zhang, Y. Liu and L. Hao, Contributions of open crop straw burning emissions to PM2. 5 concentrations in China, *Environ. Res. Lett.*, 2016, **11**, 014014.
20 Y. Zhou, Z. Han, R. Liu, B. Zhu, J. Li and R. Zhang, A modeling study of the impact of crop residue burning on PM2. 5 concentration in Beijing and Tianjin during a severe autumn haze event, *Aerosol Air Qual. Res.*, 2018, **18**, 1558–1572.
21 Z. Cheng, S. Wang, X. Fu, J. G. Watson, J. Jiang, Q. Fu, C. Chen, B. Xu, J. Yu and J. C. Chow, Impact of biomass burning on haze pollution in the Yangtze River delta, China: a case study in summer 2011, *Atmos. Chem. Phys.*, 2014, **14**, 4573–4585.
22 D. Luo, L. Luo, N. Wang, J. Wu and L. Liu, Impact of Open Crop Straw Biomass Burning Emissions on the Air Pollution in the Hunan Province, China: A Case Study, *Aerosol Sci. Eng.*, 2025, 1–17.
23 G. He, T. Liu and M. Zhou, Straw burning, PM2. 5, and death: Evidence from China, *J. Dev. Econ.*, 2020, **145**, 102468.
24 H. Yao, Y. Song, M. Liu, S. Archer-Nicholls, D. Lowe, G. McFiggans, T. Xu, P. Du, J. Li and Y. Wu, Direct radiative effect of carbonaceous aerosols from crop residue burning during the summer harvest season in East China, *Atmos. Chem. Phys.*, 2017, **17**, 5205–5219.
25 L. Chen, Y. Gao, M. Ma, L. Wang, Q. Wang, S. Guan, X. Yao and H. Gao, Striking impacts of biomass burning on PM2. 5 concentrations in Northeast China through the emission inventory improvement, *Environ. Pollut.*, 2023, **318**, 120835.
26 L. Huang, Y. Zhu, Q. Wang, A. Zhu, Z. Liu, Y. Wang, D. T. Allen and L. Li, Assessment of the effects of straw burning bans in China: Emissions, air quality, and health impacts, *Sci. Total Environ.*, 2021, 789.
27 R. Gao, W. Jiang, W. Gao and S. Sun, Emission inventory of crop residue open burning and its high-resolution spatial distribution in 2014 for Shandong province, China, *Atmos. Pollut. Res.*, 2017, **8**, 545–554.
28 J. Wu, S. Kong, F. Wu, Y. Cheng, S. Zheng, Q. Yan, H. Zheng, G. Yang, M. Zheng and D. Liu, Estimating the open biomass burning emissions in central and eastern China from 2003 to 2015 based on satellite observation, *Atmos. Chem. Phys.*, 2018, **18**, 11623–11646.
29 J. D. Fast, W. I. Gustafson Jr, R. C. Easter, R. A. Zaveri, J. C. Barnard, E. G. Chapman, G. A. Grell and S. E. Peckham, Evolution of ozone, particulates, and aerosol direct radiative forcing in the vicinity of Houston using a fully coupled meteorology-chemistry-aerosol model, *J. Geophys. Res. Atmos.*, 2006, **111**, D21305.
30 G. A. Grell, S. E. Peckham, R. Schmitz, S. A. McKeen, G. Frost, W. C. Skamarock and B. Eder, Fully coupled "online" chemistry within the WRF model, *Atmos. Environ.*, 2005, **39**, 6957–6975.
31 W. C. Skamarock, J. B. Klemp, J. Dudhia, D. O. Gill, D. M. Barker, M. G. Duda, X.-Y. Huang, W. Wang and J. G. Powers, *A Description of the Advanced Research WRF Version 3, Report NCAR/TN-475+STR*, National Center for Atmospheric Research, Boulder, Colorado, 2008.
32 Y. Zhang, Online-coupled meteorology and chemistry models: history, current status, and outlook, *Atmos. Chem. Phys.*, 2008, **8**, 2895–2932.
33 G. Geng, Y. Liu, Y. Liu, S. Liu, J. Cheng, L. Yan, N. Wu, H. Hu, D. Tong and B. Zheng, Efficacy of China's clean air actions to tackle PM2. 5 pollution between 2013 and 2020, *Nat. Geosci.*, 2024, **17**, 987–994.
34 M. Li, H. Liu, G. Geng, C. Hong, F. Liu, Y. Song, D. Tong, B. Zheng, H. Cui and H. Man, Anthropogenic emission inventories in China: a review, *Natl. Sci. Rev.*, 2017, **4**, 834–866.
35 J. Hu, L. Huang, M. Chen, H. Liao, H. Zhang, S. Wang, Q. Zhang and Q. Ying, Premature Mortality Attributable to Particulate Matter in China: Source Contributions and Responses to Reductions, *Environ. Sci. Technol.*, 2017, **51**, 9950–9959.
36 Y. Zheng, Q. Zhang, D. Tong, S. J. Davis and K. Caldeira, Climate effects of China's efforts to improve its air quality, *Environ. Res. Lett.*, 2020, **15**, 104052.
37 M. Li, Q. Zhang, J.-i. Kurokawa, J.-H. Woo, K. He, Z. Lu, T. Ohara, Y. Song, D. G. Streets and G. R. Carmichael, MIX: a mosaic Asian anthropogenic emission inventory under the international collaboration framework of the MICS-Asia and HTAP, *Atmos. Chem. Phys.*, 2017, **17**, 935–963.
38 A. Guenther, X. Jiang, C. L. Heald, T. Sakulyanontvittaya, T. a. Duhl, L. Emmons and X. Wang, The Model of Emissions of Gases and Aerosols from Nature version 2.1 (MEGAN2. 1): an extended and updated framework for modeling biogenic emissions, *Geosci. Model Dev.*, 2012, **5**, 1471–1492.
39 L. K. Emmons, R. H. Schwantes, J. J. Orlando, G. Tyndall, D. Kinnison, J. F. Lamarque, D. Marsh, M. J. Mills, S. Tilmes, C. Bardeen, R. R. Buchholz, A. Conley, A. Gettelman, R. Garcia, I. Simpson, D. R. Blake, S. Meinardi and G. Pétron, The Chemistry Mechanism in the Community Earth System Model Version 2 (CESM2), *J. Adv. Model. Earth Syst.*, 2020, **12**, e2019MS001882.
40 Y. Zhou, X. Xing, J. Lang, D. Chen, S. Cheng, L. Wei, X. Wei and C. Liu, A comprehensive biomass burning emission

inventory with high spatial and temporal resolution in China, *Atmos. Chem. Phys.*, 2017, **17**, 2839–2864.

41 Y. Zhou, Y. Zhang, B. Zhao, J. Lang, X. Xia, D. Chen and S. Cheng, Estimating air pollutant emissions from crop residue open burning through a calculation of open burning proportion based on satellite-derived fire radiative energy, *Environ. Pollut.*, 2021, **286**, 117477.

42 Y. Wu, Y. Han, A. Voulgarakis, T. Wang, M. Li, Y. Wang, M. Xie, B. Zhuang and S. Li, An agricultural biomass burning episode in eastern China: Transport, optical properties, and impacts on regional air quality, *J. Geophys. Res. Atmos.*, 2017, **122**, 2304–2324.

43 X. Huang, A. Ding, L. Liu, Q. Liu, K. Ding, X. Niu, W. Nie, Z. Xu, X. Chi, M. Wang, J. Sun, W. Guo and C. Fu, Effects of aerosol–radiation interaction on precipitation during biomass-burning season in East China, *Atmos. Chem. Phys.*, 2016, **16**, 10063–10082.

44 C. Emery, Z. Liu, A. G. Russell, M. T. Odman, G. Yarwood and N. Kumar, Recommendations on statistics and benchmarks to assess photochemical model performance, *J. Air Waste Manage. Assoc.*, 2017, **67**, 582–598.

45 C. Emery, E. Tai and G. Yarwood, *Enhanced Meteorological Modeling and Performance Evaluation for Two Texas Ozone Episodes*, Prepared for the Texas natural resource conservation commission, ENVIRON International Corporation, 2001, p. 161.

46 WorldPop, *China 1km Population, UN-adjusted*, DOI: 10.5258/SOTON/WP00671, accessed 14 August, 2025.

47 R. Chen, P. Yin, X. Meng, C. Liu, L. Wang, X. Xu, J. A. Ross, L. A. Tse, Z. Zhao and H. Kan, Fine particulate air pollution and daily mortality. A nationwide analysis in 272 Chinese cities, *Am. J. Respir. Crit. Care Med.*, 2017, **196**, 73–81.

48 X. He, Q. Huang, D. Yang, Y. Yang, G. Xie, S. Yang, C. Liang and Z. Qin, Spatiotemporal Analysis of Open Biomass Burning in Guangxi Province, China, from 2012 to 2023 Based on VIIRS, *Fire*, 2024, **7**, 370.

49 Q. Lv, Z. Yang, Z. Chen, M. Li, B. Gao, J. Yang, X. Chen and B. Xu, Crop residue burning in China (2019–2021): Spatiotemporal patterns, environmental impact, and emission dynamics, *Environ. Sci. Ecotechnology*, 2024, **21**, 100394.

50 J. Liang, S. Pan, N. Xia, W. Chen and M. Li, Threshold response of the agricultural modernization to the open crop straw burning CO2 emission in China's nine major agricultural zones, *Agric. Ecosyst. Environ.*, 2024, **368**, 109005.

51 N. You, J. Dong, J. Huang, G. Du, G. Zhang, Y. He, T. Yang, Y. Di and X. Xiao, The 10-m crop type maps in Northeast China during 2017-2019, *Sci. Data*, 2021, **8**, 41.

52 Z. Yao, X. Zheng, B. Xie, B. Mei, R. Wang, K. Butterbach-Bahl, J. Zhu and R. Yin, Tillage and crop residue management significantly affects N-trace gas emissions during the non-rice season of a subtropical rice-wheat rotation, *Soil Biol. Biochem.*, 2009, **41**, 2131–2140.

53 Z. Yu, F. Li, W. Si and W. Zhang, From Agri-Waste to Sustainable Use: A Case Study of Straw Management Reform in Northeast China, *Sustain. Dev.*, 2024, **33**, 3818–3830.

54 X. Yang, L. Cheng, X. Huang, Y. Zhang, C. Yin and P. Lebailly, Incentive mechanism to promote corn stalk return sustainably in Henan, China, *Sci. Total Environ.*, 2020, **738**, 139775.

55 Y. Xie, Z. Li, H. Zhong, X. L. Feng, P. Lu, Z. Xu, T. Guo, Y. Si, J. Wang and L. Chen, Short-Term ambient particulate air pollution and hospitalization expenditures of cause-specific cardiorespiratory diseases in China: a multicity analysis, *Lancet Reg. Health West. Pac.*, 2021, **15**, 100232.

56 J. Gao, B. Zhu, H. Xiao, H. Kang, C. Pan, D. Wang and H. Wang, Effects of black carbon and boundary layer interaction on surface ozone in Nanjing, China, *Atmos. Chem. Phys.*, 2018, **18**, 7081–7094.

57 R. Tang, X. Huang, D. Zhou and A. Ding, Biomass-burning-induced surface darkening and its impact on regional meteorology in eastern China, *Atmos. Chem. Phys.*, 2020, **20**, 6177–6191.

58 Y. Xie, L. Zeng, S. Hu, T. Wang, Z. Du, T. Tan, N. Xu, S. Chen, J. Mao and F. Xu, Long-term trends of black carbon levels, sources, and radiative effects from 2013 to 2022 in Beijing, China, *npj Clean Air*, 2025, **1**, 10.